Physics-Informed Neural Network for Nonlinear Structural System Identification

TONG LIU and HADI MEIDANI

ABSTRACT

Structural system identification is a critical task in resilience assessments, especially following a natural hazard. In this paper, we propose PIDynNet, a novel physics-informed approach that produces an ordinary differential equation-constrained neural network model for structural system identification. PIDynNet improves the estimation of structural parameters of nonlinear structural systems by embedding an auxiliary physics-based loss term into the overall loss function as well as a supervised data-driven loss term. The proposed framework has the generalization capability to predict nonlinear structural response given unseen ground excitations. Two nonlinear numerical experiments are conducted to demonstrate the advantage of PIDynNet over other identification methods in problems with or without latent variables.

INTRODUCTION

Structural health monitoring (SHM) is a critical task in the life-cycle assessment and reliability analysis of civil infrastructure systems. Structural system identification (SSI) is one of the essential components of structural health monitoring in which the parameters of the mathematical model of the structural response are estimated. SSI can also be used to identify damages in civil infrastructure systems including buildings [1] and bridges [2]. Pervasive and versatile SSI algorithms have been proposed over the past decades and can be categorized into time domain versus frequency domain methods, and parametric versus non-parametric approaches (for theoretical foundation and comprehensive surveys see [3]).

Time-domain SSI methods include restoring forces surface (RFS), sparse identification of nonlinear dynamics (SINDy), Kalman Filter-based approach, and computer vision-based approach. RFS method approximates the surface with a polynomial series or parametric expression using the measured response [4, 5]. The drawback of the RFS method is that it requires more terms for non-smooth nonlinear cases [6]. The SINDy

Tong Liu, Ph.D. student, Email: tongl5@illinois.edu. Department of Civil and Environmental Engineer- ing, University of Illinois at Urbana-Champaign, Urbana, IL, USA. Hadi Meidani, associate professor, Email: meidani@illinois.edu. Department of Civil and Environmental Engineering, University of Illinois at Urbana-Champaign, Urbana, IL, USA.

approach approximates the dynamics equation by a sparse polynomial representation, using the least absolute shrinkage and selection operator method [7]. Kalman Filter has also been used in system identification and state estimation using incoming measurement data, state equations and a noise model [8,9]. Additionally, computer vision-based identification methods have been proposed to exploit videos captured from structure's vibration using drones and other high-resolution cameras by tracking inter-frame pixel changes [10, 11].

Furthermore, the machine learning and artificial neural network (ANN) have been recently demonstrated as promising tools in many complex problems in civil engineering [12, 13]. ANN applications in structural engineering are mainly threefold: dynamic response prediction, structural system identification, and structural damage detection and localization [14]. However, machine learning models require large datasets to reach the state-of-the-art performance. One approach is to integrate model-guided constraints to compensate for data insufficiency. It does so by considering a physics-based loss function, which is in the form of the residual of the governing differential equations. Physics-informed training has been successfully used for deterministic and random differential equations [15–17]. Recent study [18] shows that neural networks with physics-based loss have the potential to be effectively used for structural modeling and model updating.

However, these works didn't treat structural system identification and structural response prediction simultaneously under the same framework, and the generalization capability of the trained neural network for structural response prediction wasn't studied thoroughly. To address the aforementioned issues, we develop PIDynNet, an ode-constrained neural network for nonlinear structure system identification, and show applications to identify structural parameters under earthquake excitations. Meanwhile, we can use the same architecture to predict the structural system response under different earthquake scenarios.

METHODOLOGY

Physics informed neural network

The goal of PINN is to train a neural network to approximate the solution of the ODE with given initial conditions. The loss function used in training measures how well the neural network approximation satisfies the governing equation and initial conditions. Consider a general ODE with an approximation solution $\boldsymbol{u}(t, \boldsymbol{p}; \boldsymbol{\theta})$:

$$\begin{aligned} &\mathcal{N}(t, \boldsymbol{p}, \boldsymbol{u}(t, \boldsymbol{p}; \boldsymbol{\theta})) = 0, \quad t \in [0, T], \boldsymbol{p} \in \mathbb{R}^d, \\ &\mathcal{I}(0, \boldsymbol{p}, \boldsymbol{u}(0, \boldsymbol{p}; \boldsymbol{\theta})) = 0, \quad \boldsymbol{p} \in \mathbb{R}^d, \end{aligned} \tag{1}$$

where $\mathcal{N}(\cdot)$ is a general differential operator, $\boldsymbol{\theta}$ represent the neural network parameters of the approximate solution, $t \in [0, T]$ represents the time domain, $\boldsymbol{p} \in \mathbb{R}^d$ denotes the random input parameters, and $\mathcal{I}(\cdot)$ denotes the initial conditions. To estimate the approximated solution, i.e. to find the neural network parameters $\boldsymbol{\theta}$, we form the following residual-based loss terms:

$$
\begin{aligned}
r_{\mathcal{N}}(\boldsymbol{\theta}) &\approx \frac{1}{N_L}\sum_{i=1}^{N_L}\mathcal{N}(t_i, \boldsymbol{p}_i, \boldsymbol{u}_i; \boldsymbol{\theta})^2, \\
r_{\mathcal{I}}(\boldsymbol{\theta}) &= \mathcal{I}(t_0, \boldsymbol{p}_0, \boldsymbol{u}_0; \boldsymbol{\theta})^2,
\end{aligned} \tag{2}
$$

where N_L is the number of collocation points. The network parameters $\boldsymbol{\theta}$ can then be estimated by minimizing a weighted loss function as follows:

$$
\boldsymbol{\theta}^* = \underset{\boldsymbol{\theta}}{\operatorname{argmin}}\; w_{\mathcal{N}} r_{\mathcal{N}}(\boldsymbol{\theta}) + w_{\mathcal{I}} r_{\mathcal{I}}(\boldsymbol{\theta}), \tag{3}
$$

where $w_{\mathcal{N}}$ and $w_{\mathcal{I}}$ denote the assigned weights for each loss term. This loss function consists of derivatives with respect to time which is an explicit input to the neural network approximation of the response and therefore these derivatives can be efficiently calculated using backpropagation.

Structural system identification

Structural system identification is an inverse problem with a forward model typically in the form of a forced multiple degrees of freedom (MDOF) linear dynamical systems with the following general form:

$$
\boldsymbol{M}\ddot{\boldsymbol{x}}(t) + \boldsymbol{C}\dot{\boldsymbol{x}}(t) + \boldsymbol{K}\boldsymbol{x}(t) = \boldsymbol{f}\left(t\right), \tag{4}
$$

where $\boldsymbol{M}, \boldsymbol{C}, \boldsymbol{K} \in \mathbb{R}^{N\times N}$ denote the mass, damping, and inter-story stiffness matrices, respectively, $\boldsymbol{x}^T = [x_1, \ldots, x_N]^T$, $\dot{\boldsymbol{x}}^T = [\dot{x}_1, \ldots, \dot{x}_N]^T$, and $\ddot{\boldsymbol{x}}^T = [\ddot{x}_1, \ldots, \ddot{x}_N]^T$ are displacement, velocity and acceleration vectors of the N-degree of freedom system, and $\boldsymbol{f} = [f_1, \ldots, f_N]^T$ is the external force on each degree of freedom. The type of external force can be ground excitations, wind load, etc. Given a ground excitation, Eq. 4 can be rewritten in the following form:

$$
\boldsymbol{M}\ddot{\boldsymbol{x}}(t) + \boldsymbol{C}\dot{\boldsymbol{x}}(t) + \boldsymbol{K}\boldsymbol{x}(t) = -\boldsymbol{M}\vec{\boldsymbol{1}}\ddot{x}_g\left(t\right). \tag{5}
$$

The objective of structural system identification is to determine the structural parameter $\boldsymbol{\theta}_p = \{\boldsymbol{C}, \boldsymbol{K}\}$. In a single degree of freedom (SDOF) system under ground excitation, the Eq. 5 will be simplified as:

$$
m\ddot{x}(t) + c\dot{x}(t) + kx(t) = -m\ddot{x}_g(t), \tag{6}
$$

where $\boldsymbol{\theta}_p = \{c, k\}$ are damping and stiffness coefficients that are estimated in the system identification process.

PIDynNet for nonlinear structural system identification

The framework of the proposed PIDynNet is shown in Figure 1. It consists of two parts: a response prediction network (RPN) and a parameter identification model. The input of the RPN, $\boldsymbol{I} = \{\boldsymbol{t}, \ddot{\boldsymbol{x}}_g\}$, consists of sampled times $\boldsymbol{t}$ and ground accelerations at those times $\ddot{\boldsymbol{x}}_g(t)$. The task of RPN is to predict the response, by mapping the input vector into the output vector $\tilde{\boldsymbol{x}}$, e.g., $\boldsymbol{x} = \mathrm{RPN}(\boldsymbol{I}; \boldsymbol{\theta}_R)$, where $\boldsymbol{\theta}_R$ denotes the trainable weights and biases in RPN. Then the output of RPN is passed into an automatic

differentiator. By taking the first and second derivatives with respect to time, the outputs including approximated velocity and accelerations, denoted by $\boldsymbol{S} = \{\dot{\tilde{\boldsymbol{x}}}, \ddot{\tilde{\boldsymbol{x}}}\}$, are calculated.

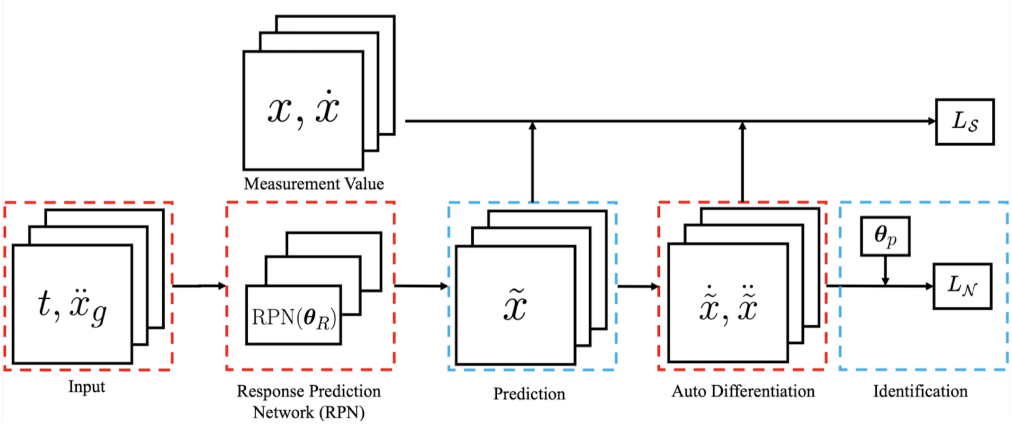

Figure 1. The framework of PIDynNet with RPN.

The system identification is accomplished by simultaneously learning the structural parameters $\boldsymbol{\theta}_p$ and neural network parameters $\boldsymbol{\theta}_R$ simultaneously by solving the following optimization problem:

$$\boldsymbol{\theta}_R^*, \boldsymbol{\theta}_p^* = \underset{\boldsymbol{\theta}_R, \boldsymbol{\theta}_p}{\operatorname{argmin}} \quad w_{\mathcal{N}} L_{\mathcal{N}}(\boldsymbol{\theta}_R, \boldsymbol{\theta}_p) + w_{\mathcal{S}} L_{\mathcal{S}}(\boldsymbol{\theta}_R), \tag{7}$$

where $w_{\mathcal{N}}$, $w_{\mathcal{S}}$ are weight parameters for the physics-based $L_{\mathcal{N}}$ and supervised loss functions $L_{\mathcal{S}}$, respectively. For instance, the physics-based loss term for the SDOF system governed by Eq. 6, where $\boldsymbol{\theta}_p = [c, k]$, is given by:

$$L_{\mathcal{N}}(\boldsymbol{\theta}_R, \boldsymbol{\theta}_p) = \mathbb{E}_{\boldsymbol{I}\sim p(\boldsymbol{I})}\left[L_{\mathcal{N}}\left(\boldsymbol{\theta}_R, \boldsymbol{\theta}_p | \boldsymbol{I}\right)\right] \approx \sum_{i=1}^{N_L} \left\| m\ddot{\tilde{\boldsymbol{x}}}^i(\boldsymbol{\theta}_R) + c\dot{\tilde{\boldsymbol{x}}}^i(\boldsymbol{\theta}_R) + k\tilde{\boldsymbol{x}}^i(\boldsymbol{\theta}_R) + m\ddot{\boldsymbol{x}}_g^i \right\|_2^2. \tag{8}$$

This physics-based loss will encourage the identified structural parameters and the predicted response to conform simultaneously to the governing equations. The supervised loss function is given by:

$$L_{\mathcal{S}}(\boldsymbol{\theta}_R) = \mathbb{E}_{\boldsymbol{I}\sim p(\boldsymbol{I})}\left[L_{\mathcal{S}}\left(\boldsymbol{\theta}_R | \boldsymbol{x}, \dot{\boldsymbol{x}}, \boldsymbol{I}\right)\right] \approx \sum_{i=1}^{N_L} \left\| \tilde{\boldsymbol{x}}^i(\boldsymbol{\theta}_R) - \boldsymbol{x}^i \right\|_2^2 + \sum_{i=1}^{N_L} \left\| \dot{\tilde{\boldsymbol{x}}}^i(\boldsymbol{\theta}_R) - \dot{\boldsymbol{x}}^i \right\|_2^2. \tag{9}$$

This term measures the difference between the neural network prediction and the ground truth signal. Instead of minimizing the loss function by using data from the whole response time period, PIDynNet seeks to minimize the loss function by sequentially training the network and structural parameters over consecutive subperiods. Specifically, the subperiods are created by equally dividing the whole response time period. Then, using data from each subperiod, PIDynNet is trained and the structural parameters are calculated, and serve as the initial values in the next subperiod. Within each subperiod,

there are variabilities in the calculated parameters over the iterations of the algorithm. As more subperiods are used, one expects these variabilities to get reduced. Thus we require the structural parameters in the next subperiod to be constrained in the range $\{\boldsymbol{p}^* - 3\boldsymbol{\sigma_p}, \boldsymbol{p}^* + 3\boldsymbol{\sigma_p}\}$, where $\boldsymbol{p}^*$ is the latest estimate for the parameters, and $\boldsymbol{\sigma_p}$ is the standard deviation of the parameters that are estimated through iterations in the current subperiod. During the iteration in the training process, the value of identified parameters is checked every N_c iteration, and an early stopping strategy is introduced if the unknown parameters $\boldsymbol{\theta}_p$ doesn't change beyond the threshold ϵ for n successive evaluation starting from iteration N_0:

$$\left\|\boldsymbol{\theta}_p^{N_0+iN_c} - \boldsymbol{\theta}_p^{N_0}\right\| / \left\|\boldsymbol{\theta}_p^{N_0}\right\| < \epsilon \quad \forall i = 1, \ldots, n. \tag{10}$$

Dynamical systems with latent state variables

Dynamical systems with rate-dependent behavior can pose a challenge for system identification since the system is now governed by multiple differential equations with additional latent rate-dependent variables. Let us consider the following general form for a rate-dependent dynamical system:

$$\begin{cases} m\ddot{\boldsymbol{x}}(t) + f(\Phi(\boldsymbol{x}), \Psi(\boldsymbol{z}); \boldsymbol{\theta}_p) = -m\ddot{x}_g(t) \\ \dot{\boldsymbol{z}} = g(x, z; \boldsymbol{\theta}_z) \end{cases}, \tag{11}$$

where $f(\cdot)$ is a function controlling the restoring force, Φ, Ψ are dictionaries containing all related variables, $g(\cdot)$ is the function controlling the rate-dependent behavior characterizing by parameter $\boldsymbol{\theta}_z$. In order to predict the additional latent variables in PIDynNet, we train the latent neural network (LNN), where the predictions are $\tilde{\boldsymbol{z}}$ = LNN($\boldsymbol{I}; \boldsymbol{\theta}_L$), with $\boldsymbol{\theta}_L$ being the weights and biases in LNN. So, the physics-informed loss term $L_{\mathcal{Z}}$ is given by:

$$L_{\mathcal{Z}}(\boldsymbol{\theta}_R, \boldsymbol{\theta}_L, \boldsymbol{\theta}_z) = \sum_{i=1}^{N} \left\|\dot{\tilde{\boldsymbol{z}}}^i(\boldsymbol{\theta}_L) - g\left(\tilde{\boldsymbol{x}}^i(\boldsymbol{\theta}_R), \tilde{\boldsymbol{z}}^i(\boldsymbol{\theta}_L); \boldsymbol{\theta}_z\right)\right\|_2^2, \tag{12}$$

where $\dot{\tilde{\boldsymbol{z}}}^i$ and other derivatives in $g(\cdot)$, are calculated using automatic differentiation of LNN. Therefore, the parameter optimization with latent variable is given by:

$$\boldsymbol{\theta}_R^*, \boldsymbol{\theta}_L^*, \boldsymbol{\theta}_p^*, \boldsymbol{\theta}_z^* = \underset{\boldsymbol{\theta}_R, \boldsymbol{\theta}_L, \boldsymbol{\theta}_p, \boldsymbol{\theta}_z}{\operatorname{argmin}} \quad w_{\mathcal{N}} L_{\mathcal{N}}(\boldsymbol{\theta}_R, \boldsymbol{\theta}_p) + w_{\mathcal{S}} L_{\mathcal{S}}(\boldsymbol{\theta}_R) + w_{\mathcal{Z}} L_{\mathcal{Z}}(\boldsymbol{\theta}_R, \boldsymbol{\theta}_L, \boldsymbol{\theta}_z). \tag{13}$$

The workflow of modified PIDynNet is shown in Figure 2. The network make prediction on $\tilde{\boldsymbol{x}}$ and latent variable $\tilde{\boldsymbol{z}}$ separately then aggregate all the variables in the loss function with unknown parameters.

Generalization capability of PIDynNet

After identifying the unknown structural model using the response to a given record, the neural network can be generalized to predict the response time history under an unseen ground excitation. For an unseen ground motion, we just re-train the PIDynNet

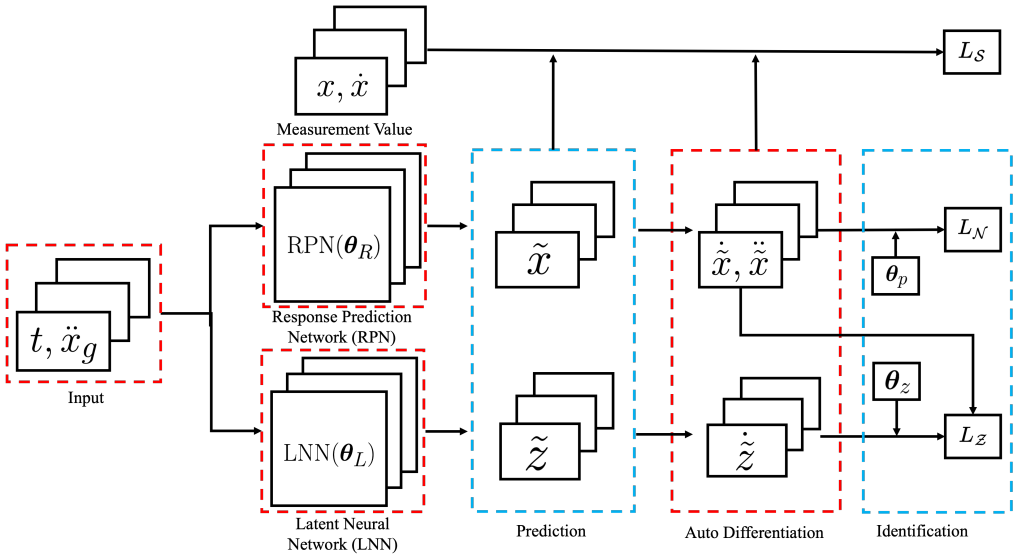

Figure 2. Modified framework of PIDynNet with RPN and LNN.

for a few 'fine-tuning' steps. During the fine-tuning process, the structural parameters, θ_p and θ_z, are kept fixed and only the neural network parameters, θ_R and θ_L, are re-trained. This fine-tuning is not supervised training, and only uses physics-based loss functions. So the fine-tuning loss function in the case without latent variables is given by:

$$\boldsymbol{\theta}_R^{**} = \underset{\boldsymbol{\theta}_R}{\text{argmin}} \; L_{\text{fine-tuning}}(\boldsymbol{\theta}_R, \boldsymbol{\theta}_p^*) = \underset{\boldsymbol{\theta}_R}{\text{argmin}} \; w_{\mathcal{N}} L_{\mathcal{N}}(\boldsymbol{\theta}_R, \boldsymbol{\theta}_p^*). \tag{14}$$

NUMERICAL RESULTS

SDOF cubic stiffness system

The proposed PIDynNet framework is first validated on a highly nonlinear structural system with cubic stiffness, which is also known as the Duffing system. In particular, the Duffing oscillator can be interpreted as a forced oscillator with nonlinear (3^{rd} order) elastic stiffeners whose restoring force is written as:

$$m\ddot{x}(t) + c\dot{x}(t) + k_1 x(t) + k_3 x^3(t) = -m\ddot{x}_g(t), \tag{15}$$

where k_1, k_3 are the parameters governing the restoring force. In our example, the system parameters are set as $m = 1\text{kg}$, $c = 0.5\text{N} \cdot \text{s/m}$, $k_1 = 15\text{N/m}$, $k_3 = 120\text{N/m}^3$. The natural frequency of the system is 3.87 Hz when the effect of the nonlinear term is negligible. The Kobe Earthquake ground motion from Pacific Earthquake Engineering Research Center (PEER) ground motion database is used. A scaled version of the 40-second ground motion record is adopted to let the response spectrum match with the target spectrum within the range of $0.2T_1$ to $1.5T_1$, where T_1 is the first mode structural period. The training data, which includes displacement, velocity, and acceleration time histories, are obtained from the third-order Runge-Kutta Method.

In the identification process, the initial learning rate is set as 0.001, and the number of collocation points is 500 from a sampling pool size of 1000 for each subperiod. The subperiod length is 3s. The early stopping strategy for parameters is evaluated for every 100 iterations with the threshold of 10^{-4}. A pretraining process for RPN with 1000 iterations is performed before the identification with only supervised loss in order to have better initialization of θ_R values. The maximum number of iterations in each subperiod is set to be 80,000. The architecture of RPN is a five-layer multi-layer perceptron. The embedding size of the hidden layer is 32. All the loss terms are equally weighted in training process.

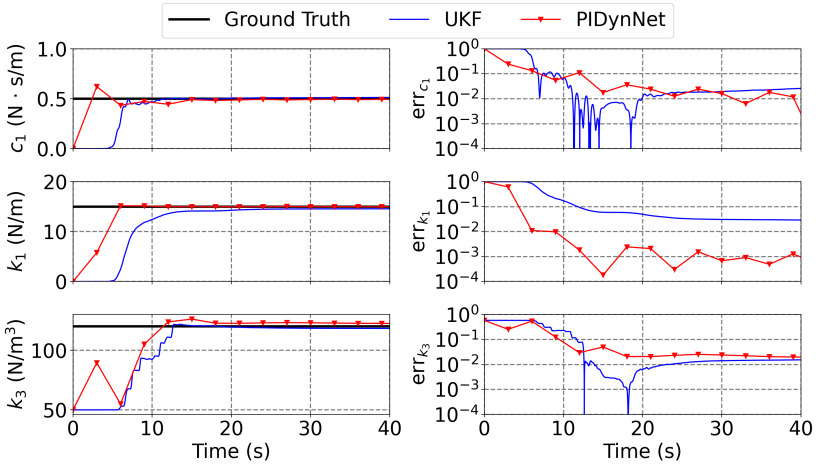

Figure 3. Comparison of parameter updating results and errors on SDOF duffing system.

TABLE I. The errors in the identified parameters with batch size of 400.

Parameter	Ground truth value	UKF value	UKF error	PIDynNet velue	PIDynNet error (%)
$c_1(\mathrm{N}\cdot\mathrm{s/m})$	0.5	0.513	2.86	0.494	**1.19**
$k_1(\mathrm{N/m})$	15	14.564	2.91	14.981	**0.13**
$k_3(\mathrm{N/m^3})$	120	118.164	**1.53**	122.392	1.99

The identified result from the PIDynNet is compared with the ground truth and also with results from the unscented Kalman filter (UKF). Figure 3 shows the comparison of identification results from PIDynNet with ground truth and UKF identification value. Both approaches cannot identify the parameters in the first 5 seconds since the structural response is small and has not exhibited nonlinear behaviors. When the system starts to exhibit nonlinear behavior, the structural parameters in the identification block of PIDynNet start to converge to the ground truth to minimize the physics-informed loss. Figures in the left column indicate that PIDynNet has a faster convergence speed compared to UKF. And the right column presents the relative error of different parameters. Table I compares the identified modal parameters obtained from PIDynNet and UKF after the last time step. The largest estimation error by PIDynNet is 1.99 % while the largest error by UKF is 2.91 %. It indicates that PIDynNet offers a relatively better prediction than UKF.

As discussed earlier, a trained PIDynNet can also be used for structural response prediction, and here we seek to assess the generalization capability of the response prediction of PIDynNet. Several unseen excitations are generated by scaling and stretching

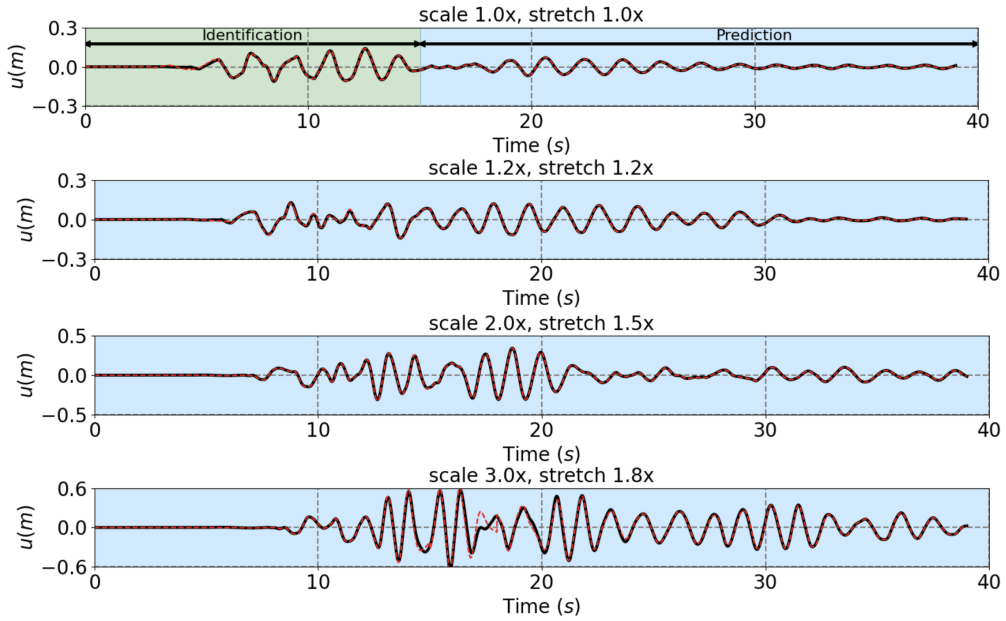

Figure 4. Identification and prediction results of nonlinear displacements under different magnitudes and distribution of correlation coefficient in cubic stiffness system.

the original ground motion record used in the identification phase. Figure 4 shows the identification and prediction result of unseen excitations. The green region shows an identification phase, from $t = 0$s to $t = 15$s. The blue regions indicate the prediction phase, where the PIDynNet predicts the response time history under unseen ground excitations. To measure the similarity between the reference and the prediction, the Pearson correlation coefficient γ is computed to quantify the fitness of the predicted response with respect to the ground truth signals. The histogram in 5 presents the distribution of the correlation coefficient under different ground motions and different scales. We observed that about 95% of the prediction responses have a correlation coefficient $\gamma \geq 0.95$.

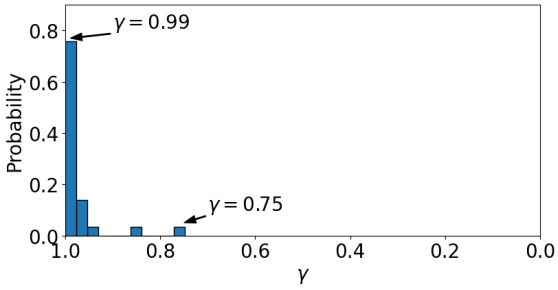

Figure 5. Distribution of correlation coefficient under different ground motions.

SDOF Bouc-Wen Model

In this example, PIDynNet is applied on a SDOF Bouc-Wen system. Bouc-Wen model is one of the widely used hysteretic models originally proposed by Bouc [19] and later developed by Wen [20]. The latent hysteretic displacement in the restoring force

has dynamics which is dependent on the structure's velocity. The governing differential equations under ground excitation are then given by

$$\begin{cases} m\ddot{x}(t) + c\dot{x}(t) + kz(t) = -\ddot{x}_g(t), \\ \dot{z}(t) = \dot{x}(t) - \gamma |\dot{x}(t)| |z(t)|^{n-1} z(t) - \beta \dot{x}(t) |z(t)|^n, \end{cases} \tag{16}$$

where c and k are damping and stiffness coefficient. z is the latent hysteretic displacement, and β, γ, and n are dimensionless parameters that control the hysteretic behavior, and can generate a large variety of hysteretic loops. For this example, since the latent hysteretic displacements are unobserved, one can expect the training of LNN to be slow. Thus, we adopt a transfer learning-based initialization, where after pretraining the RPN, we transfer the parameters from RPN into the LNN. Furthermore, to account for the discrepancy between hysteretic displacement from structural displacement, the difference between the initial displacement and initial hysteretic displacement is added to the output of LNN. The initial structural displacements and initial hysteretic displacements in each subperiod are computed from its previous subperiod.

TABLE II. Identification result of SDOF Bouc-Wen Model with noise-free data

Parameter	Ground Truth	UKF	Error (%)	PIDynNet	Error (%)
$c(\mathrm{N}\cdot\mathrm{s/m})$	0.3	0.286	4.58	0.295	**1.50**
$k(\mathrm{N/m})$	12	11.987	**0.11**	11.954	0.38
β	1.0	0.988	**1.25**	0.982	1.77
γ	2.0	2.051	2.57	1.963	**1.87**
n	2.0	2.064	3.21	2.051	**2.57**

In this example, the system parameters are set as $m = 1\mathrm{kg}$, $c = 0.3\mathrm{N}\cdot\mathrm{s/m}$, $k = 12\mathrm{N/m}$, $\beta = 1$, $\gamma = 2$, $n = 2$. The natural frequency of the system is 0.55 Hz. The identification process and hyperparameters are identical to the previous case study. The El Centro Earthquake ground motion from the PEER dataset is used. Table II compares the accuracies in the identified parameters of the Bouc-Wen model. The average identification error by PIDynNet is 1.68 % and the average error by UKF is 2.25 %. Additionally, the largest estimation error by PIDynNet is 2.57 % while the largest error by UKF is 4.58%, underscoring the overall better performance of PIDynNet.

TABLE III. Comparison of computed parameters of the Bouc-Wen model identified using UKF and PIDynNet with respect to the ground truth under different noise levels.

Parameter	Ground Truth	2.5% Noise				5% Noise			
		UKF	Error (%)	PIDynNet	Error (%)	UKF	Error (%)	PIDynNet	Error (%)
$c(\mathrm{N}\cdot\mathrm{s/m})$	0.3	0.292	2.53	0.301	**0.37**	0.316	5.49	0.294	**1.84**
$k(\mathrm{N/m})$	12	12.016	**0.13**	12.032	0.27	11.956	0.36	11.987	**0.11**
β	1.0	0.975	2.49	1.017	**1.72**	0.971	2.86	1.027	**2.70**
γ	2.0	2.022	**1.08**	1.952	2.41	1.948	2.58	1.950	**2.50**
n	2.0	1.960	2.02	1.989	**0.56**	2.064	3.18	2.020	**1.02**

In order to assess the robustness of the model, similar to the previous case study, different measurement noise levels are considered. And the results in Table III show the

comparison of identified parameters of the Bouc-Wen model using UKF and PIDynNet under different noise levels. The PIDynNet model has yielded an average identification error of less than 1.75% at both noise levels. In contrast, the UKF model has exhibited a prediction error greater than 50% as compared to PIDynNet. It indicates that PIDynNet can offer relatively accurate identification even for noisy data, with an average identification error lower than that of UKF.

CONCLUSION

The paper presents PIDynNet, a novel ode constrained structural identification framework with neural networks. In particular, the ode constrained neural network utilizes the physics-based loss, to identify the unknown structural parameters. Along with supervised loss, the physics-based loss is embedded in the overall loss function, which is considered an auxiliary constraint to enforce the architecture to capture the dynamic response within the feasible space. Besides, the PIDynNet is successful in identifying the parameters when the system consists of non-observable nonlinear state variables. In addition to identification, the PIDynNet shows the generalization capability when encountering unseen earthquakes.

For validation, the performances of ode constrained neural network were tested on two numerical examples: (1) an SDOF system with 3^{rd} order hardening stiffness, (2) an SDOF Bouc-Wen Model. The ode constrained neural network is successful in identifying the modal parameters and outperforms other data-driven identification methods. The prediction results with unseen earthquakes indicate that PIDynNet has the generalization capability. It is believed that the ode constrained neural network provides a large variety of implementation fields and promising potentials for structural health monitoring.

ACKNOWLEDGMENT

This material is based in part upon work supported by the National Science Foundation under Grant No. CMMI-1752302 and USDOT under Grant No. 69A3551747105.

REFERENCES

1. Abazarsa, F., S. Ghahari, F. Nateghi, and E. Taciroglu. 2013. “Response-only modal identification of structures using limited sensors,” *Structural Control and Health Monitoring*, 20(6):987–1006.
2. Eshkevari, S. S., T. J. Matarazzo, and S. N. Pakzad. 2020. “Bridge modal identification using acceleration measurements within moving vehicles,” *Mechanical Systems and Signal Processing*, 141:106733.
3. Sirca Jr, G. and H. Adeli. 2012. “System identification in structural engineering,” *Scientia Iranica*, 19(6):1355–1364.
4. Allen, M. S., H. Sumali, and D. S. Epp. 2008. “Piecewise-linear restoring force surfaces for semi-nonparametric identification of nonlinear systems,” *Nonlinear Dynamics*, 54(1-2):123–135.

5. Villani, L. G., S. Da Silva, and A. Cunha. 2020. "Application of a stochastic version of the restoring force surface method to identify a Duffing oscillator," in *Nonlinear Dynamics of Structures, Systems and Devices*, Springer, pp. 299–307.
6. Ceravolo, R., S. Erlicher, and L. Z. Fragonara. 2013. "Comparison of restoring force models for the identification of structures with hysteresis and degradation," *Journal of Sound and Vibration*, 332(26):6982–6999.
7. Leylaz, G., S. F. Ma, and J.-Q. Sun. 2021. "An Optimal Model Identification Algorithm of Nonlinear Dynamical Systems With the Algebraic Method," *Journal of Vibration and Acoustics*, 143(2).
8. Mu, H.-Q. and K.-V. Yuen. 2015. "Novel outlier-resistant extended Kalman filter for robust online structural identification," *Journal of Engineering Mechanics*, 141(1):04014100.
9. Karimi, P., M. Butala, and F. Kamalabadi. 2020. "Efficient model selection in switching linear dynamic systems," *arXiv preprint arXiv:2012.04543*.
10. Oh, B. K., J. W. Hwang, Y. Kim, T. Cho, and H. S. Park. 2015. "Vision-based system identification technique for building structures using a motion capture system," *Journal of Sound and Vibration*, 356:72–85.
11. Zhou, Y., L. Zhang, T. Liu, and S. Gong. 2018. "Structural system identification based on computer vision," *China Civil Engineering Journal*, 51(11):17–23.
12. Zou, D., M. Zhang, Z. Bai, T. Liu, A. Zhou, X. Wang, W. Cui, and S. Zhang. 2022. "Multicategory damage detection and safety assessment of post-earthquake reinforced concrete structures using deep learning," *Computer-Aided Civil and Infrastructure Engineering*, 37(9):1188–1204.
13. Liu, T. and H. Meidani. 2023. "Optimizing Seismic Retrofit of Bridges: Integrating Efficient Graph Neural Network Surrogates and Transportation Equity," in *Proceedings of Cyber-Physical Systems and Internet of Things Week 2023*, pp. 367–372.
14. Salehi, H. and R. Burgueño. 2018. "Emerging artificial intelligence methods in structural engineering," *Engineering structures*, 171:170–189.
15. Psichogios, D. C. and L. H. Ungar. 1992. "A hybrid neural network-first principles approach to process modeling," *AIChE Journal*, 38(10):1499–1511.
16. Nabian, M. A. and H. Meidani. 2019. "A deep learning solution approach for high-dimensional random differential equations," *Probabilistic Engineering Mechanics*, 57:14–25.
17. Raissi, M., P. Perdikaris, and G. E. Karniadakis. 2019. "Physics-informed neural networks: A deep learning framework for solving forward and inverse problems involving nonlinear partial differential equations," *Journal of Computational Physics*, 378:686–707.
18. Zhang, R., Y. Liu, and H. Sun. 2020. "Physics-informed multi-LSTM networks for metamodeling of nonlinear structures," *Computer Methods in Applied Mechanics and Engineering*, 369:113226.
19. Bouc, R. 1967. "Forced vibrations of mechanical systems with hysteresis," in *Proc. of the Fourth Conference on Nonlinear Oscillations, Prague, 1967*.
20. Wen, Y.-K. 1976. "Method for random vibration of hysteretic systems," *Journal of the engineering mechanics division*, 102(2):249–263.